Photochemical & Photobiological Sciences (2022) 21:2139–2151
https://doi.org/10.1007/s43630-022-00284-2

ORIGINAL PAPERS

Selective aqueous oxidation of aromatic alcohols under solar light in the presence of TiO_2 modified with different metal species

Marianna Bellardita[1] · Mansoor Feilizadeh[2] · Roberto Fiorenza[3] · Salvatore Scirè[3] · Leonardo Palmisano[1] · Vittorio Loddo[1]

Received: 2 May 2022 / Accepted: 31 July 2022 / Published online: 21 August 2022

Abstract

A set of metals modified TiO_2 photocatalysts were prepared starting from titanium tetraisopropoxyde and different metal precursors to study the influence of the addition of the various foreign agents on the physico-chemical and photocatalytic properties of the catalysts. The powders were characterized by X-ray diffraction, Raman spectroscopy, specific surface area measurements, scanning electron microscopy, energy dispersive X-ray spectroscopy, UV–Vis diffuse reflectance spectroscopy, photoluminescence, temperature programmed desorption after CO_2 adsorption. The photocatalytic activity was evaluated using as probe reactions the partial oxidation of three aromatic alcohols: benzyl alcohol (BA), 4-methoxy benzyl alcohol (4-MBA), and 4-hydroxy benzyl alcohol (4-HBA) under simulated solar light irradiation. Different oxidation and selectivity values were obtained for the three substrates depending not only on the type of metals but also on the nature and position of the substituent in the phenyl ring of benzyl alcohol. As a general behaviour, the doped samples allowed the achievement of a greater selectivity especially for 4-MBA even if sometimes with minor conversions. The presence of W or Nb was beneficial for both conversion and selectivity for all the substrates with respect to bare TiO_2.

Graphical abstract

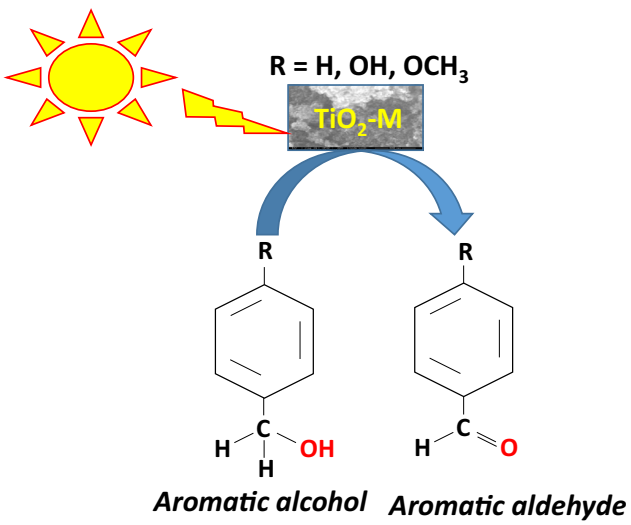

Keywords TiO_2 · Aromatic alcohols · Selective oxidation · Simulated solar light

✉ Marianna Bellardita
marianna.bellardita@unipa.it

Extended author information available on the last page of the article

1 Introduction

In the past, heterogeneous photocatalysis has been mainly proposed for environmental depollution as it allows to obtain a complete mineralization and disappearance of many toxic organic and inorganic species that are present in both liquid and gaseous effluents [1]. However, in more recent years its ability to selectively oxidize some organic molecules into others with high added value has been highlighted, through the appropriate choice of experimental conditions and photocatalysts. This indicates that this technology can be an ecological and sustainable alternative to industrial catalytic processes [2, 3, 4, 5, 6, 7].

The photocatalytic process can also be considered economical because it works at ambient conditions often using water as a solvent and non-toxic species as oxidizing agents. In particular, this technology becomes competitive when sunlight is used as a source of irradiation. A valid strategy to achieve this goal is the loading/doping of TiO_2, the most studied photocatalyst, with metal or non-metal species [8, 9, 10] and/or the coupling with other semiconductors forming heterojunctions [11, 12, 13, 14]. In fact, the efficiency of the photocatalytic process is often low in the presence of bare TiO_2, due to the quite high recombination rate of the photoproduced electrons and holes, while the above reported strategies can improve the separation of photogenerated charges.

The selective oxidation of aromatic alcohols to the corresponding aldehydes is a key reaction in the field of organic syntheses that has been carried out, in some cases with high yields, in the presence of TiO_2-based photocatalysts in organic solvents [15, 16] and in water [17, 6]. The use of water as a solvent in the laboratory and on an industrial scale is highly desirable even if the selectivity may be lower than that obtained in the presence of organic solvents.

Many parameters related both to the catalyst features (crystalline phase, hydroxylation and crystallinity degree, amount of photo produced OH radicals, presence of surface acidic or basic sites, crystalline facet, presence of ions in solution) and the substrate chemical properties (presence and position of substituent in the aromatic ring) can influence the photocatalytic activity. It is generally difficult to directly correlate the photocatalytic activity to a single property of the catalysts, and the substrate-photocatalyst interaction should also be considered. Only in very few cases few properties can be directly related to photoactivity. For example, for the photodegradation of some aliphatic and aromatic acids with different acid strengths, TiO_2 photocatalysts doped with various metal species which gave the surface a very different acidity showed different activity. The main properties addressing the photoactivity were the dissociation constants (K_a) of the acids used as substrates and the points of zero charge (PZC) of the photocatalysts [18]. In the case of the hydroxylation of phenol and benzoic acid, instead, the selectivity toward mono-hydroxy derivatives showed a strong dependence on catalyst hydroxylation and crystallinity degrees of the different TiO_2 photocatalysts: the highest selectivity values were obtained using the least hydroxylated and the most crystalline samples [19]. Moreover, the photoactivity of various commercial and laboratory-produced TiO_2 samples, which exhibited a different degree of crystallinity and surface density of OH, was compared for the degradation of 4-nitrophenol and the partial oxidation of 4-methoxybenzyl alcohol to 4-methoxybenzaldehyde [20]. The most crystalline samples showed the highest activity for 4-nitrophenol degradation whereas the least crystalline and most hydroxylated catalysts were the most active for the selective oxidation of 4-methoxybenzyl alcohol. Thanks to an EPR study, these results were attributed to the fact that not all the surface hydroxyl groups were capable of generating hydroxyl radicals under irradiation [20]. The same research group also observed that the high photoactivity of TiO_2 samples prepared in HF solutions for 2-propanol total oxidation and 4-methoxybenzyl alcohol selective oxidation, was prevalently due to the presence of fluorine rather than to the exposure of specific TiO_2 facets [21].

The aim of this work was to study the partial aqueous oxidation of some aromatic alcohols to the corresponding aldehydes under simulated solar light irradiation in the presence of different home-made TiO_2-based samples. In particular, catalysts consisting of TiO_2 doped/loaded with different metal species have been synthetized with the aim of modifying the surface and bulk characteristics of the bare titanium dioxide. The photocatalytic activity was correlated with some properties of the photocatalysts and with the structure of the substrate. Although numerous studies have been conducted in recent years, the role of the different parameters that affect the TiO_2 photoactivity has not yet been fully understood.

2 Experimental

2.1 Samples preparation

Bare TiO_2 was prepared by adding 29 ml of titanium(IV) isopropoxide (TTIP) to an ethanolic solution obtained with 230 ml of ethanol, 27 ml of H_2O, 4 ml of HCl, and 5.5 g of Pluronic F127. A white suspension was obtained and held 24 h at 313 K to evaporate the solvent. The final solid was dried 24 h at 383 K and subsequently calcined 24 h at 773 K. For the preparation of loaded/doped TiO_2 an amount of metallic salts corresponding to a nominal 1% w/w of metal

with respect to TiO_2 was added to the ethanolic solution before the addition of TTIP. Namely, CuCl, $NiCl_2$, $CeCl_3$, $NbCl_5$, WCl_6, and $MgCl_2$ were used as metal precursors.

2.2 Samples characterization

The samples were physicochemically characterized by means of different techniques. X-ray diffraction (XRD) patterns were acquired at room temperature by a PANalytical Empyrean diffractometer equipped with a PIXcel1D (tm) detector working at a voltage of 40 kV and a current of 40 mA and using the CuK_α radiation with a 2θ scan rate of 1.28°/min. The relative amount of anatase and rutile was determined by the following equations [22, 23, 24]:

$$W_A = \frac{0.886 \cdot A_A}{0.886 \cdot A_A + A_R}, \quad (1)$$

$$W_R = \frac{A_R}{0.886 \cdot A_A + A_R}, \quad (2)$$

where A_A and A_R represent the integrated intensity of the anatase (1 0 1) peak (2θ = 25.3°), and the rutile (1 1 0) one (2θ = 27.5°), respectively.

The average crystallites size of the synthetized powders was calculated by applying the Scherrer formula using the (1 0 1) anatase and (1 1 0) rutile diffraction peaks.

Raman spectra were recorded in the 125–800 cm^{-1} Raman shift range by a BwTek i-Raman plus system equipped with a 785 nm laser focalized on the sample by means of a microscope equipped with a 20 × magnification lens. The signal integration time was 5 s and each spectrum was the average of 2 repetitions.

Specific surface area (SSA) of the powders was measured by a FlowSorb 2300 instrument (Micromeritics) using the single-point BET method. Before the measurements, the samples were degassed by a N_2/He mixture 30/70 (v/v) for 0.5 h at 523 K.

Diffuse reflectance spectra (DRS) were acquired by a Shimadzu UV-2401 PC spectrophotometer in the 200–800 nm wavelength range, using $BaSO_4$ as the reference material. Band gap values were determined by plotting the modified Kubelka–Munk function, $[F(R'_\infty)h\nu]^{1/2}$, vs the energy of the exciting light.

Scanning electron microscopy (SEM) images were acquired by means of a FEI Quanta 200 ESEM microscope operating at 30 kV. An electron microprobe used in an energy dispersive mode (EDX) was used to obtain information on samples composition.

Photoluminescence (PL) spectra were obtained at room temperature by means of a Horiba Jobin Yvon spectrofluorometer (FluoroMax-4) using an excitation energy of 300 nm.

The TPD (Temperature Programmed Desorption) measurements of the samples in the presence of adsorbed CO_2 were carried out in a fixed bed quartz reactor containing 150 mg of samples. After the CO_2 adsorption and the surface saturation processes, the CO_2 flow (30 cc/min) was stopped. Then the reactor was heated from 50 to 600 °C at a rate of 10 °C/min. The desorption peaks were examined with a Sensorlab VG Quadrupoles mass spectrometer. Before the measurements, the samples were flushed in He (30 cc/min) for 1 h at 250 °C to avoid other adsorption processes.

2.3 Photocatalytic runs

The photocatalytic activity of the powders was evaluated in a liquid–solid–gas Pyrex cylindrical batch reactor containing 150 mL of 0.5 mM aqueous solution of the different alcohols. In particular, the partial oxidation of three aromatic alcohols: benzyl alcohol (BA), 4-methoxy benzyl alcohol (4-MBA), and 4-hydroxy benzyl alcohol (4-HBA) has been evaluated. An axially placed 100 W halogen lamp (radiant power, measured by a radiometer Delta Ohm DO9721, ca. 20 W m^{-2} and ca. 0.5 W m^{-2} in the 450–900 nm and 315–400 nm ranges, respectively) was used as the irradiation source. The runs were carried out for 4 h and the reactor was open to atmospheric air. A Pyrex cooling jacket allowed, through the circulation of water, the maintenance of the reaction temperature at about 28 °C. During the runs, samples of the irradiated suspension were withdrawn at fixed times, and filtered through 0.25 μm membranes (PTFE, Whatman) to separate the photocatalyst particles. A Beckman Coulter HPLC instrument equipped with a Diode Array detector was used to determine the concentration of the substrate and its oxidation products by a Phenomenex KINETEK 5 μm C18 100A column (4.6 × 150 mm) working at room temperature; the eluent (0.8 mL min^{-1}) consisted of a mixture (20:80 v:v) of acetonitrile and 13 mM trifluoroacetic acid aqueous solution. The various substrates were analysed at different wavelengths relative to their adsorption spectra: benzyl alcohol and benzaldehyde at 210 nm, 4-methoxy benzyl alcohol at 230 nm, 4-methoxybenzaldehyde at 260 nm, 4-hydroxy benzyl alcohol and 4-hydroxybenzaldehyde at 220 nm.

2.4 Quantum efficiency determination

The energetic efficiency of the heterogeneous photocatalytic system can be determined by evaluating two quantities: (i) the rate of photon absorption (rpa) and (ii) the specific reaction rate (srr):

$$rpa = \frac{\text{number of absorbed photons}}{\text{time} \cdot \text{surface area}} \left[\frac{Einstein}{s \cdot m^2}\right], \quad (3)$$

$$srr = \frac{\text{number of reacted molecules}}{\text{time} \cdot \text{surface area}} \left[\frac{moles}{s \cdot m^2}\right]. \quad (4)$$

Both these rates should be evaluated on the basis of the active sites but this last quantity is very difficult to be experimentally determined, and then the BET surface area can be used as approximated parameter of reference. From the experimental determination of rpa and srr, the quantum efficiency can be found and used to compare different photocatalysts:

$$\eta = \frac{\text{number of reacted molecules}}{\text{number of absorbed photons}}. \quad (5)$$

The number of absorbed photons was determined by neglecting the diffusion and/or reflection phenomena and considering only the photon emitted by the lamp (φ_i) and the photons transmitted by the dispersion (φ_t). Then the absorbed photons (φ_a) can be calculated by the following equation:

$$\phi_a = \phi_i - \phi_t. \quad (6)$$

To have the maximum exploit of the photons emitted by the lamp, the optimum amount of photocatalyst was determined by adding quantities of the powder in the reacting solution and measuring the transmitted flow at the external wall of the reactor. When the transmitted flow reached the 10% of the emitted one the value of the weight of the solid was chosen. A value not null of the transmitted flow assured us that all the catalyst was irradiated thus avoiding shielding effects.

φ_i was measured by filling the reactor with water and measuring, by means of a radiometer, its value at the external wall of the reactor. The lamp used was a quartz halogen one whose emission spectrum resembles that reported in Fig. 1.

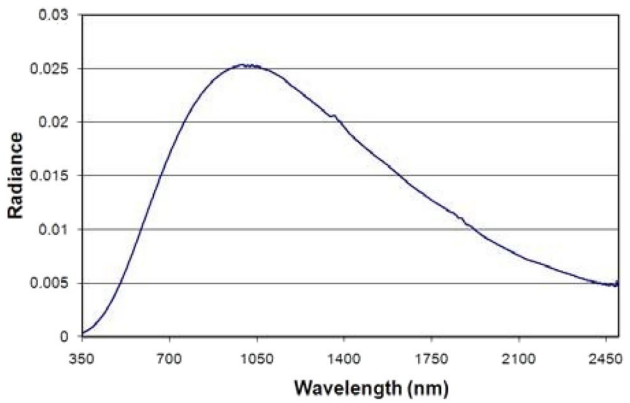

Fig. 1 Emission spectrum of the used lamp

Two photocells were used for the measurements of the emitted and transmitted flows, one for the range 315–400 nm (ϕ_{i1}, ϕ_{t1}) and the other for the range 450–900 nm (ϕ_{i2}, ϕ_{t2}).

$$\begin{aligned} \phi_{i1} &= 20\, W/m^2 \quad \phi_{i2} = 0.5\, W/m^2, \\ \phi_{t1} &= 2\, W/m^2 \quad \phi_{t2} = 0.05\, W/m^2. \end{aligned} \quad (7)$$

To convert W/m^2 in Einst/s, the Planck equation was used. The energy of a photon at a certain wavelength is:

$$E[J] = \frac{h[J \cdot s] \cdot c\left[m \cdot s^{-1}\right]}{\lambda[m]}. \quad (8)$$

In which h is the Planck constant and C the light speed. For a mol of photons (1 Einstein) it should be multiplied for the Avogadro number

$$1\text{Einst} = \text{E} \cdot \text{N}_\text{A}. \quad (9)$$

By considering the average values of the two wavelength ranges (i.e. $\lambda_1 = 575$ and $\lambda_2 = 375.5$ nm) the following energies of the photons were calculated:

$$E_1 = \frac{6.626 \cdot 10^{-34}[J \cdot s] \cdot 3^8\left[m \cdot s^{-1}\right]}{575 \cdot 10^{-9}[m]} = 3.457 \cdot 10^{-19}\ \text{J},$$

$$E_2 = \frac{6.626 \cdot 10^{-34}[J \cdot s] \cdot 3^8\left[m \cdot s^{-1}\right]}{375.5 \cdot 10^{-9}[m]} = 5.294 \cdot 10^{-19}\ \text{J}. \quad (10)$$

They correspond to the following energies of one mol of photons:

$$\begin{aligned} Einst_1 &= 6.022^{23} \cdot 3.457 \cdot 10^{-19} = 2.082 \cdot 10^5\ \text{J}, \\ Einst_2 &= 6.022^{23} \cdot 5.294 \cdot 10^{-19} = 3.188 \cdot 10^5\ \text{J}. \end{aligned} \quad (11)$$

Thus:

$$\begin{aligned} \phi_{a1} &= \phi_{i1} - \phi_{t1} = 20 - 2 = 18\, W/m^2 = 8.9 \cdot 10^{-5}\, Einst/s, \\ \phi_{a2} &= \phi_{i2} - \phi_{t2} = 0.5 - 0.05 = 0.45\, W/m^2 = 1.411 \cdot 10^{-6}\, Einst/s. \end{aligned} \quad (12)$$

Therefore, the rate of photon absorption is:

$$\phi_a = \phi_{a1} + \phi_{a2} = 8.901 \cdot 10^{-5} Einst/s \cdot m^2. \quad (13)$$

The ssr can be written as:

$$ssr = -r = \frac{1}{S}\frac{dN}{dt} = \frac{V}{S}\frac{dC}{dt} = k \ \text{(the reaction order is zero)}, \quad (14)$$

$$\frac{dC}{dt} = \frac{S}{V}k, \quad (15)$$

$$C = C_0 - \frac{S}{V}kt. \quad (16)$$

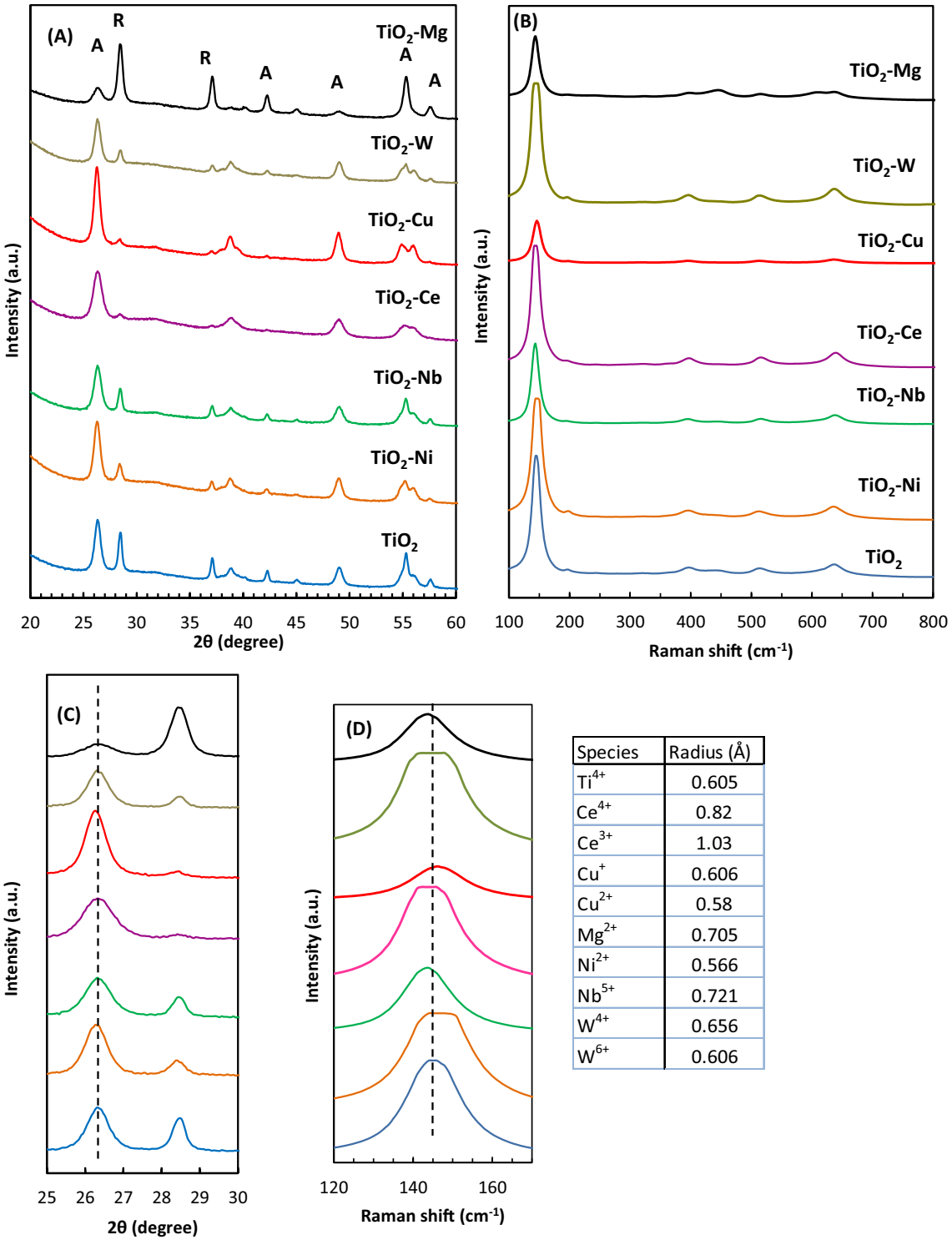

Species	Radius (Å)
Ti^{4+}	0.605
Ce^{4+}	0.82
Ce^{3+}	1.03
Cu^{+}	0.606
Cu^{2+}	0.58
Mg^{2+}	0.705
Ni^{2+}	0.566
Nb^{5+}	0.721
W^{4+}	0.656
W^{6+}	0.606

Fig. 2 XRD patterns (**A**) and Raman spectra (**B**) of the used samples. **C** Enlargement of the anatase XRD peak at 2θ = 25 degree; **D** Enlargement of the anatase Raman peak at 144 cm^{-1}. *A* Anatase; *R* Rutile

By applying a least square best fitting procedure to the experimental data the values of k were determined.

3 Results and discussion

XRD patterns of bare and differently doped TiO_2 samples are presented in Fig. 2A. The pristine catalyst prevalently consisted of anatase phase (main peaks at $2\theta = 25.5°$, 38.0°, 48.0°, 54.5°) with a minor amount of rutile one (main peaks at $2\theta = 27.5°$, 36.5°, 41°, 54.1°, 56.5°). The addition of metal species did not change the samples composition but a different distribution of anatase and rutile can be noticed (Table 1). In particular, a decrease in the rutile fraction was observed with the exception of Mg, being in this case the rutile amount higher than that present in the other samples. As reported in the literature, the presence of metal ions during the crystallization of TiO_2 can hinder the growth of a crystalline phase and favour that of another [23]. For example, the preparation of TiO_2 samples in the presence of fluoride ions revealed the formation of anatase instead of rutile and brookite, which were obtained under the same experimental conditions but in the absence of fluorides [25].

A little influence was, instead, noticed on the crystallites size in the presence of the different metals. No peaks associated to the different metals can be observed due to their low amount and high dispersion degree on the TiO_2 surface.

In Fig. 2B, the Raman spectra of the used samples are reported. The vibrational modes of anatase at 144 cm^{-1} (Eg), 196 cm^{-1} (Eg), 397 cm^{-1} (B1g), 513 cm^{-1} (A1g), and 639 cm^{-1} (B1g) and rutile at 447 (Eg) and 612 (A1g) cm^{-1} can be observed. In the presence of the metal species, the spectra are very similar to those of bare TiO_2, and no new peaks are present confirming the good dispersion of the dopants as indicated also by XRD diffractograms. Nevertheless, it is possible to notice, on the basis of the particular dopant, an intensity variation. Specifically, the intensity of the peak at 144 cm^{-1} was higher than that observed for bare TiO_2 after the addition of W, Ce, and Ni and the most significant reduction occurred in the presence of Cu. The reduction of the Raman peak intensity was usually attributed to the presence of oxygen vacancies [26].

Additionally, by enlarging the main anatase XRD peak at 25° (Fig. 2C), a little shift to lower degrees is observable only in the presence of Ni and Cu. In accordance with [27] this can be attributed to the introduction of a relevant part of these ions into the TiO_2 lattice due also to the similarity of their ionic radii with that of Ti^{4+}. Notably, the ionic radii of Cu^{2+} and Ni^{2+} are among the metals studied the only ones smaller than that of Ti^{4+}. The other metals, probably, are prevalently present on the TiO_2 surface and/or in interstitial position.

By enlarging the Raman Eg peak at 144 cm^{-1} (see Fig. 2D), in fact, a small shift can be seen in the presence of the different metals suggesting their insertion into the TiO_2 lattice [28, 29]. Relating to the anatase TiO_2 strongest Eg mode, it is reported that a shift towards higher wave numbers is related to oxygen vacancies [30], whilst a shift towards lower wave numbers can be associated with a lattice distortion as this band derives from the O–Ti–O band vibration [27, 31]. In our case a shift to higher wave number is observed only with Ni and Cu, in the presence of which also a shift in the XRD anatase main peak was observed. It is worth remembering that by replacing Ti^{4+} ions with species such as Cu^{2+} and Ni^{2+} which possess a lower oxidation state, can induce the formation of some oxygen vacancies.

Specific surface area (SSA) of bare TiO_2 was 73 $m^2\ g^{-1}$ (Table 1). The presence of foreign species had generally a little influence on the surface area value, but a considerable increase was noticed only for TiO_2–Ce.

Table 1 Specific surface area (BET) and band-gap (E_g), crystalline phase *A* Anatase and *R* Rutile, crystallite size (φ), and Ti, O and metal weight EDX percentages of the catalysts studied

Sample	S_{BET} (m^2/g)	E_g (eV)	Crystalline phase	φ (nm)	Ti (w/w%)	O (w/w%)	Metal (w/w%)
TiO_2	73	2.96	A (69) R (31)	A (11.9) R (23.8)	54.55	45.45	–
TiO_2–Ni	74	2.78	A (83) R (17)	A (10.9) R (17.0)	71.31	27.10	1.59
TiO_2–Nb	75	3.00	A (74) R (26)	A (9.3) R (14.9)	58.96	40.53	0.51
TiO_2–Ce	117	2.80	A (95) R (5)	A (10.0) R (17.0)	56.70	42.62	0.68
TiO_2–Cu	85	2.76	A (96) R (4)	A (10.9) R (23.8)	59.71	39.85	0.44
TiO_2–W	79	2.96	A (84) R (16)	A (10.9) R (19.8)	59.74	39.02	1.24
TiO_2–Mg	65	2.98	A (11) R (89)	A (23.7) R (13.3)	49.30	48.54	2.16

The band-gap values, determined by plotting the modified Kubelka–Munk function, $[F(R'_{\infty})\ h\nu]^{1/2}$, versus the energy of the exciting light, are reported in Table 1. Bare TiO_2 presented a band-gap value of 2.96 eV typical of an anatase/rutile mixture. The metal addition gave rise to a moderate band-gap reduction in the case of Ni, Ce, and Cu, allowing the activation of the samples under solar light irradiation, while had no significant effect for Nb, Mg, and W.

The EDX analysis confirmed the presence of the different metals. In the last column of Table 1 is reported the metal weight percentage experimentally determined as the average of three measurements in different part of the particle surface that was generally higher that the nominal one (1%) indicating a surface enrichment of the metal species except Nb, Ce, and Cu.

The UV–Vis DRS of the various samples are presented in Fig. 3. Bare TiO_2 shows a significant light absorption in the range 400–650 nm, probably due to the formation of oxygen vacancies as indicated by the shape of the spectrum in accordance with the literature [25, 32]. The TiO_2–Nb and TiO_2–Mg samples show a reflectance almost equal to 100% at wavelength higher than 400 nm. The other samples display an enhanced absorption in the visible region with the minimum reflectance value observed for TiO_2–Ni. The spectrum of the sample containing copper shows a maximum in the reflectance at about 550 nm, typical of Cu species hosted in TiO_2 [33, 13] due to the formation of extra energy levels in the TiO_2 band gap. This finding was confirmed by the presence of a mid-gap state which in our sample is barely sketched due to the low percentage of Cu. In particular, Cu introduces *"d"* states in the band gap of TiO_2 that generates the absorption peak in the visible region.

Photoluminescence (PL) spectra allow to compare the recombination rate of the photogenerated charge carriers. In particular, the increase in the intensity is related to a higher

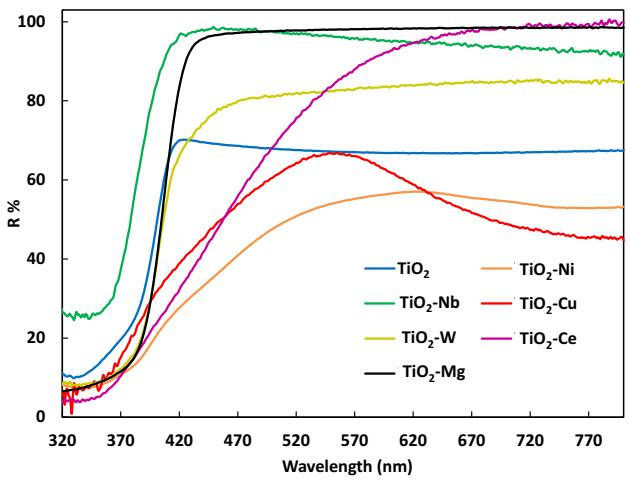

Fig. 3 DRS spectra of the different samples

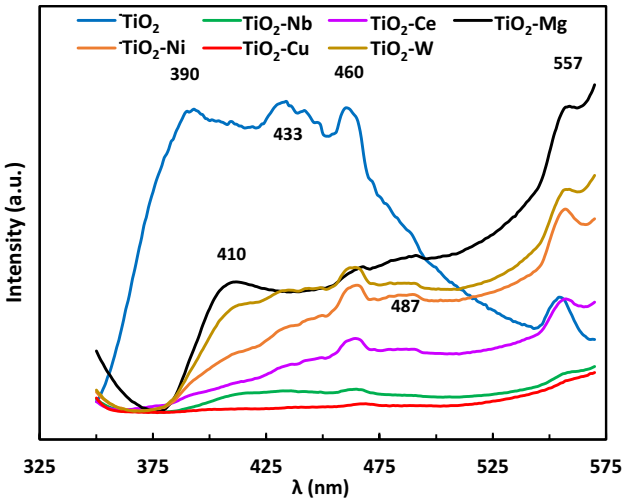

Fig. 4 Photoluminescence spectra of the examined samples

recombination between electrons and holes. The PL spectra of the examined samples are reported in Fig. 4. The bare TiO_2 sample showed four bands at about 390, 433, 460, and at 555 nm. As reported in the literature the first band was related to the band-to-band emission of TiO_2, the second one is ascribed to the excitons self-trapped in the TiO_6 octahedral structure typical of TiO_2, whereas the last two bands were related to the presence of oxygen vacancies and to the electrons trapped in the defect centres [34, 35].

Interestingly, the addition of the metals led to a significant quenching of the PL bands especially for the TiO_2–Nb

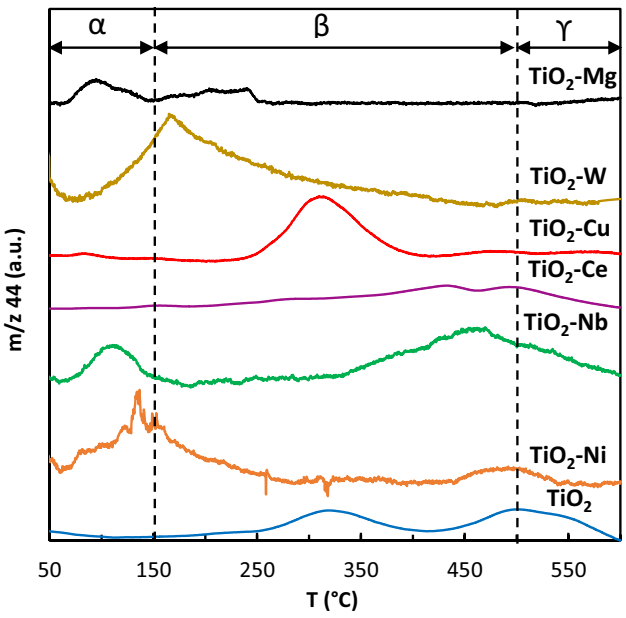

Fig. 5 CO_2-TPD curves of the used samples in the 50–600 °C temperature range

and the TiO_2–Cu samples and a shift of the band related to band-to-band emission at higher wavelengths. The decrease of the PL bands intensity is usually related to an increase of the charge carriers separation [36], therefore, the presence of the metals co-catalysts decreased the recombination rate between the electrons and the holes. The band shift can be associated to the higher absorption at higher wavelengths of metal doped/loaded samples with respect to bare TiO_2.

The strength and the modification of the basic sites of TiO_2 due to the addition of the metals were analysed by CO_2–TPD (Fig. 5). In the profiles of the samples, it is possible to discriminate among three zone: the weak basic sites (α, from 50 to 150 °C) related to the linearly adsorbed CO_2 on the surface -OH groups of the metal oxides, the medium basic sites (β, from 150 to 475 °C) and the strong basic ones (γ, from 475 to 600 °C). The peaks of these latter zones (β and γ) were characteristic of the bridge-bonded CO_2 [37, 38]. Pure TiO_2 showed only weak desorption peaks in the medium and strong basic sites zones, whereas the addition of the different metals led substantial changes. In particular, the addition of Ni, Nb, and Mg caused the formation of weak basic sites (desorption peak at about 100 °C for the TiO_2–Nb and TiO_2–Mg, whereas the TiO_2–Ni exhibited two features at about 140° and 150 °C) in accordance with the literature data [39, 40]. The TiO_2–W showed a large CO_2–TPD peak centred at around 160 °C related to the formation of further medium basic sites due to the addition of tungsten. Interestingly, the sample with copper showed a well-defined desorption peak at about 300 °C more intense compared to the same peak present in the bare TiO_2. On the contrary, the addition of Ce led to a decrease of the intensity of the desorption peaks of TiO_2. In general, the addition of metals caused the modifications of the basic sites of TiO_2 with the increase of medium, especially with the TiO_2–Cu sample, and of the weak basic sites (TiO_2–Nb, TiO_2–Ni, and TiO_2–Mg) with a progressive decrease of the strong ones. Indeed only the bare TiO_2 showed a peak in the γ zone. These findings can be explained with the occurrence of an interaction between the acidic metal species and the strong basic sites of the TiO_2 surface.

In Fig. 6 are reported the SEM images of the prepared samples. The different powders were nanostructured and consist of aggregates of small particles of irregular shape. The presence of the different metals did not influence the morphology of the samples being very similar to that of bare TiO_2.

Table 2 Alcohol conversion (*X*) and selectivity to the corresponding aldehyde (*S*) in the presence of the different catalysts

Sample	BA		4-MBA		4-HBA	
	X	S	X	S	X	S
TiO_2	23	19	32	41	24	10
TiO_2-Ni	3	75	7	94	11	7
TiO_2-Nb	36	20	36	75	16	32
TiO_2-Ce	18	19	10	100	10	30
TiO_2-Cu	15	19	6	100	8	16
TiO_2-W	37	25	32	91	33	17
TiO_2-Mg	8	90	29	67	26	10

All the runs lasted 4 h

A halogen lamp was used as irradiation source. In yellow, the result equal to that of bare TiO_2; in green values higher than that of bare TiO_2; in red values lower than that of bare TiO_2

3.1 Photoactivity results

Table 2 reports the results of the photocatalytic runs carried out under simulated solar light, in terms of alcohol conversion (*X*) and aldehyde selectivity (*S*) after 4 h of irradiation, for the three investigated starting compounds.

Alcohols conversion, *X*, and selectivity to products, *S*, have been determined as follows:

$$X = \frac{[\text{alcohol}]_i - [\text{alcohol}]_t}{[\text{alcohol}]_i} \times 100, \tag{17}$$

$$S = \frac{[\text{product}]_t}{[\text{alcohol}]_i - [\text{alcohol}]_t} \times 100, \tag{18}$$

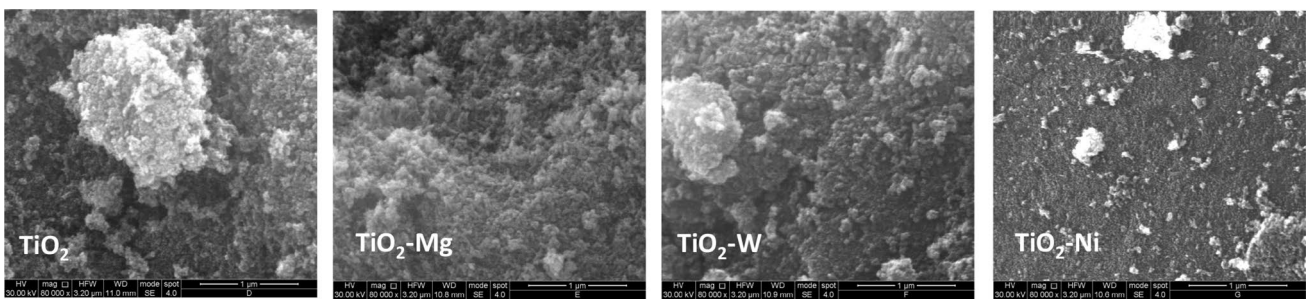

Fig. 6 SEM images of some representative samples

where $[alcohol]_i$ and $[alcohol]_t$ represent the initial molar concentration of the different alcohols and that after t time, respectively, and $[product]_t$ indicates the molar concentration of a generic product (aldehydes) after t time of irradiation.

All the prepared photocatalysts were effective in the partial oxidation of the three aromatic alcohols. For all of the substrates the selectivity and conversion values were comparable with those reported for bare TiO_2 samples under UV irradiation [41] in similar experimental conditions. The maximum measured conversion was ca. 37% and the selectivity towards the photoproduced aldehydes reached in some cases 100% for low conversion values ($\leq 10\%$). As previous observed, selectivity generally increased as conversion decreased. In the presence of the metallic species, a lower or higher oxidizing capacity was observed, but generally the selectivity was higher compared to pure TiO_2. The metallic species, however, influenced the photocatalytic behaviour differently for the three alcohols studied as substrates.

From the results of the photocatalytic tests, it is possible to conclude that the oxidizing power of the samples cannot be correlated only to the influence of metals on the electronic characteristic of the catalysts. In fact, although in their presence it can always be assumed a better separation of the photogenerated charges (see PL spectra), not all the doped/loaded photocatalysts showed a conversion of the substrates greater than that obtained with pure TiO_2. Probably this result must also be linked to changes in the acid–base properties of the surface of pure TiO_2 which influenced the substrate adsorption in different ways. In fact, the conversion reached sometimes modest values for all the alcohols and a high selectivity was measured only for 4-MBA in accordance with the literature [41, 42]. The K_a reported in literature for the three substrates studied are very low (10^{-15} for BA, $10^{-14.4}$ for 4-MBA, $10^{-9.5}$ for 4-HBA), and it is very unlikely to explain the photoactivity differences by taking into account them rather than the basic/acid sites present on the surface of the photocatalyst and/or the substituent group of the aromatic ring of the substrates (see below).

In the case of Nb and W beneficial effects were observed, and the photocatalysts showed good selectivities with a conversion greater than 30%. For the other metals, on the other hand, there was a significant reduction in the conversion with respect to bare TiO_2. These species probably also modify some of the surface properties of the catalysts used, such as the distribution of types of acidic and basic sites, hindering the adsorption of the aldehyde formed by the oxidation of alcohols, inhibiting its further decomposition and, consequently, increasing the selectivity of the reaction [43].

By comparing the behaviour of the three substrates, it is possible to note that the highest conversion and selectivity values were generally obtained by starting from 4-MBA, while the photoactivity of the catalysts studied towards BA and 4-HBA was almost the same. The different results can be explained by considering the type and position of the substituent present in the aromatic ring of benzyl alcohol.

It is reported that the presence of electron donating (ED) substituents in the para position with respect to the CH_2OH-group promotes the reactivity of the substrate without compromising the selectivity toward the benzaldehyde formation [44]. In our case this was verified for 4-MBA but not for 4-HBA, and in particular an improvement in both conversion and selectivity can be observed in the presence of the methoxy group as substituent. Hence, the conversion of alcohols cannot be related simply to the position of the substituent but also to its chemical nature and some key characteristics of the catalysts.

Another point is the behaviour of the various photocatalysts with respect to the three substrates. It is worth noting that using bare TiO_2 the degree of conversion after 4 h was the highest for 4-MBA and practically the same for BA and 4-HBA, and the behaviour after the addition of the different metals is not easy to be directly explained.

With the TiO_2–Ni sample, the conversion of all of the alcohols was very low and decreased following the order: 4-HBA > 4-MBA > BA; the presence of Nb was beneficial for the conversion of BA and 4-MBA and detrimental for 4-HBA while W increased the conversion of the alcohols with the exception of 4-MBA. The addition of the other metals was detrimental for all of the alcohols.

The partial oxidation of the alcohols gave rise mainly to the corresponding aldehydes and only trace amounts of the acids were sometimes observed, depending on the reaction time.

The perusal of Table 2 shows that also regarding the selectivity, the best results were obtained with 4-MBA. Using bare TiO_2 the maximum selectivity value (41%) was obtained for 4-methoxybenzaldehyde, although the higher alcohol conversion (32%) with respect to the other substrates. Higher selectivities were reached when the metals species were present, even if with Ni, Ce, and Cu very low conversion values were observed. On the contrary, by adding Nb, W, and Mg, the 4-MBA conversion showed little or no variations compared to that of bare TiO_2 whilst higher selectivity values were measured reaching 91% with W. Notably, in these cases, the selectivity increased although the conversion did not decrease. Using TiO_2–W, for BA and 4-HBA the selectivities to aldehyde were lower but the conversion was almost the same as for 4-MBA. This finding suggests the important role played by the interaction between the substrate and the surface of the photocatalyst, as well as the intrinsic electronic properties of the substrate.

In Fig. 7 the values of quantum efficiencies of the different photocatalysts for the three investigated substrates are compared. For all of the substrates, generally, the values of the quantum efficiency follow the trend of the photocatalytic results showed in Table 2.

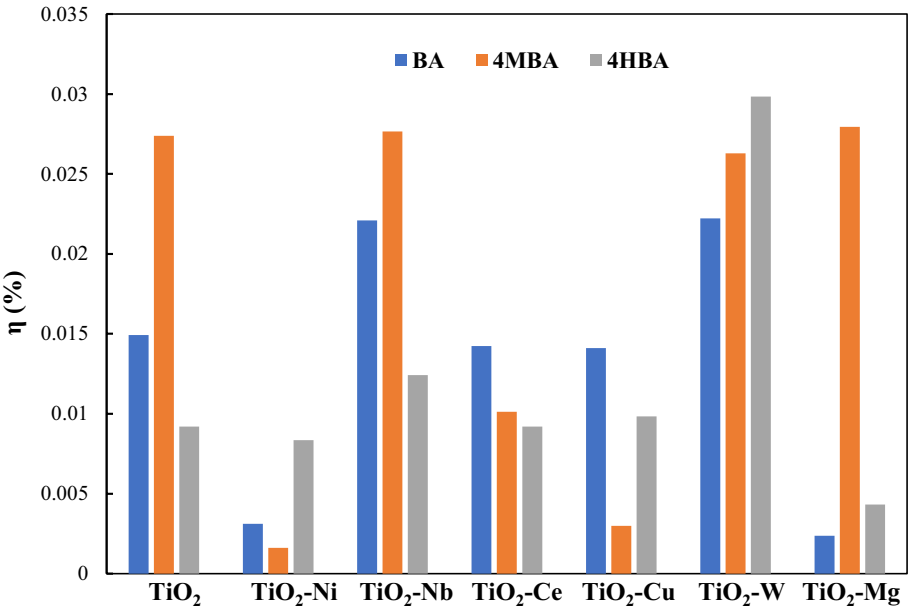

Fig. 7 Quantum efficiency of the different photocatalyst for the three substrates

The selectivity of the three alcohols (at the 15% of conversion) towards the aldehydes formed in the presence of bare TiO_2 and of the samples where the metals gave the best results is compared in the Fig. 8. With bare TiO_2 the maximum selectivity was obtained for 4-methoxybenzaldehyde, while almost the same values were found starting from the other substrates; the metal species increased the selectivity starting from 4-MBA but had a negligible influence for BA. In the presence of Nb and W, an increase and a decrease were observed, respectively, considering 4-HBA. In the case of partial oxidation of alcohols to the corresponding aldehydes, a crucial factor determining the selectivity is the desorption of the formed aldehydes from the surface of the catalyst which avoids their subsequent oxidation to carboxylic acid. In the literature it has been reported in this

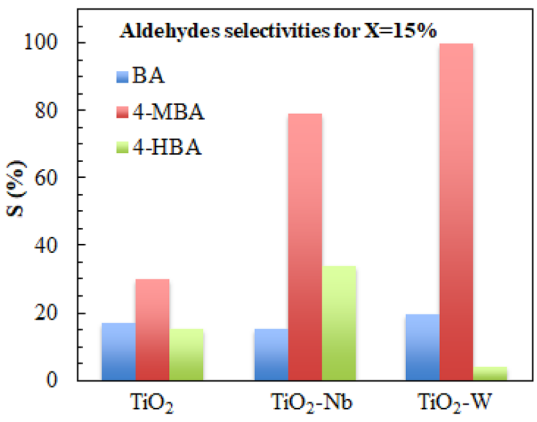

Fig. 8 Selectivity towards the different aldehydes after 15% conversion of the three alcohols in the presence of the most active photocatalysts

regards that during the formation of the vanillin from ferulic acid using TiO_2 loaded with W, the high selectivity obtained was due to the surface presence of WO_3 which hindered the subsequent oxidation–decomposition of vanillin [43].

All the doped/loaded photocatalysts displayed a lower recombination rate of the charge carriers (Fig. 4) than bare TiO_2, but only some of these displayed a higher oxidant power. The presence of the metals reduced the presence of strong basic sites, and this could be responsible for a lower interaction between the substrates and the photocatalysts surface resulting in a lower conversion and higher selectivity. However, this was not true for all the photocatalysts, and a different behaviour was noticed for the three alcohols. It is not easy to justify the results by considering only one factor, as mentioned above. Generally, even if the doping agent was present in low amount (about 1% as detected by EDX) it could modify the crystalline structure of the TiO_2 (as detected by XRD and Raman) with incorporation and/or a surface segregation. Probably the resultant photocatalytic performance is a balance of the modification of the structural properties of TiO_2 and its interaction with the substrates. The TiO_2–W and the TiO_2–Nb are the most interesting samples although they showed slight changes of the physical–chemical properties compared to the bare TiO_2. Recent studies demonstrated that the addition of Nb on TiO_2 is beneficial to have a right compromise between a good number of "positive defects" (without excessive trap levels) to increase the adsorption process [45, 46]. The presence of W, instead, allowed the formation of non-stoichiometric TiO_2 species in the surface that are beneficial for the oxidation reaction [10].

The evolution of the 4-MBA and 4-methoxybenzaldehyde (4-MBald) as a function of irradiation time in the presence of TiO_2–W is reported in Fig. 9. Throughout

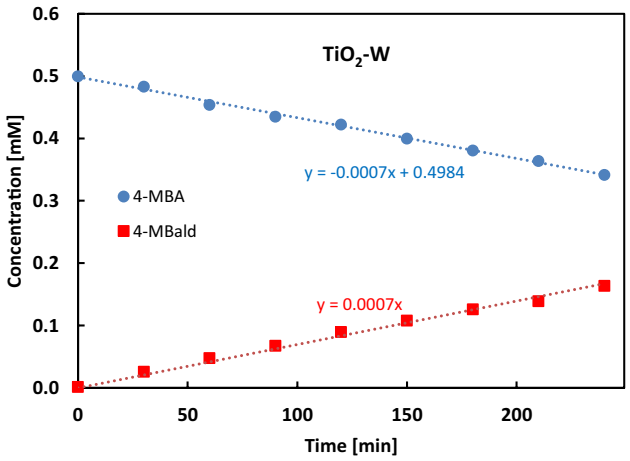

Fig. 9 Evolution of the concentration of 4-MBA and 4-MBAld versus irradiation time using TiO_2–W

the irradiation, the concentration of the initial substrate decreased and that of the formed aldehyde increased with the same rate, thus indicating a progressive transformation of the alcohol towards the aldehyde which was initially the unique product.

4 Conclusions

Bare and metal/loaded-TiO_2 samples were used for the partial oxidation of three aromatic alcohols towards the corresponding aldehydes under simulated solar light irradiation. Different conversion and selectivity values were obtained in the presence of the different metal species and a correlation between the properties of the photocatalyst and the structure of the substrate has been hypothesized, although it is very difficult to find a simple explanation for the photocatalytic activity considering only a single property of the photocatalyst. The same samples showed not only a different photoactivity towards the three tested aromatic alcohols tested but also a different trend compared to the bare TiO_2, showing in some case a positive effect, in others a negative. Usually, the photoactivity is the result of different physico-chemical and structural parameters and furthermore each photocatalyst can behave differently with different substrates due to the specific interactions between the catalyst surface and the organic compounds [47].

In our conditions, the doped samples allowed a greater selectivity especially for 4-MBA even if in some cases with lower conversions. The presence of W or Nb was beneficial both for conversion and selectivity for all the substrates with respect to bare TiO_2.

Funding Open access funding provided by Università degli Studi di Palermo within the CRUI-CARE Agreement.

Declarations

Conflict of interest On behalf of all authors, the corresponding author states that there is no conflict of interest.

References

1. Herrmann, J.-M. (1999). Heterogeneous photocatalysis: fundamentals and applications to the removal of various types of aqueous pollutants. *Catalysis Today, 53*, 115.
2. Bellardita, M., Loddo, V., & Palmisano, L. (2020). Formation of high added value chemicals by photocatalytic treatment of biomass. *Mini-Reviews in Organic Chemistry, 17*, 884–901. https://doi.org/10.2174/1570193x17666200131112856
3. Bellardita, M., Virtù, D., di Franco, F., et al. (2022). Heterogeneous photocatalytic aqueous succinic acid formation from maleic acid reduction. *Chemical Engineering Journal*. https://doi.org/10.1016/j.cej.2021.134131
4. Friedmann, D., Hakki, A., Kim, H., et al. (2016). Heterogeneous photocatalytic organic synthesis: State-of-the-art and future perspectives. *Green Chemistry, 18*, 5391–5411.
5. Kou, J., Lu, C., Wang, J., et al. (2017). Selectivity enhancement in heterogeneous photocatalytic transformations. *Chemical Reviews, 117*, 1445–1514.
6. Palmisano, L., Augugliaro, V., Bellardita, M., et al. (2011). Titania photocatalysts for selective oxidations in water. *Chemsuschem, 4*, 1431–1438.
7. Parrino, F., Bellardita, M., García-López, E. I., et al. (2018). Heterogeneous photocatalysis for selective formation of high-value-added molecules: Some chemical and engineering aspects. *ACS Catalysis, 8*, 11191–11225. https://doi.org/10.1021/acscatal.8b03093
8. Bellardita, M., Nazer, H. A. E., Loddo, V., et al. (2017). Photoactivity under visible light of metal loaded TiO_2 catalysts prepared by low frequency ultrasound treatment. *Catalysis Today, 284*, 92–99. https://doi.org/10.1016/j.cattod.2016.11.026
9. di Valentin, C., & Pacchioni, G. (2013). Trends in non-metal doping of anatase TiO2: B, C, N and F. *Catalysis Today, 206*, 12–18. https://doi.org/10.1016/j.cattod.2011.11.030
10. Fiorenza, R., Bellardita, M., Scirè, S., & Palmisano, L. (2018). Effect of the addition of different doping agents on visible light activity of porous TiO_2 photocatalysts. *Molecular Catalysis, 455*, 108–120. https://doi.org/10.1016/j.mcat.2018.06.002
11. di Credico, B., Redaelli, M., Bellardita, M., et al. (2018). Step-by-step growth of HKUST-1 on functionalized TiO_2 surface: An

efficient material for CO_2 capture and solar photoreduction. *Catalysts*. https://doi.org/10.3390/catal8090353
12. Duan, J., Zhao, H., Zhang, Z., & Wang, W. (2018). The Z-scheme heterojunction between TiO_2 nanotubes and Cu_2O nanoparticles mediated by Ag nanoparticles for enhanced photocatalytic stability and activity under visible light. *Ceramics International, 44*, 22748–22759. https://doi.org/10.1016/j.ceramint.2018.09.062
13. Fiorenza, R., Bellardita, M., Scirè, S., & Palmisano, L. (2019). Photocatalytic H_2 production over inverse opal TiO_2 catalysts. *Catalysis Today*. https://doi.org/10.1016/j.cattod.2017.12.011
14. Meng, S., Sun, W., Zhang, S., et al. (2018). Insight into the transfer mechanism of photogenerated carriers for WO_3/TiO^2 heterojunction photocatalysts: Is it the transfer of band-band or Z-scheme? why? *Journal of Physical Chemistry C, 122*, 26326–26336. https://doi.org/10.1021/acs.jpcc.8b07524
15. Mohamed, O. S., El-Aal, A., Gaber, M., & Abdel-Wahab, A. A. (2002). Photocatalytic oxidation of selected aryl alcohols in acetonitrile. *Journal of Photochemistry and Photobiology A, 148*, 205.
16. Pradhan, S. R., Nair, V., Giannakoudakis, D. A., et al. (2020). Design and development of TiO_2 coated microflow reactor for photocatalytic partial oxidation of benzyl alcohol. *Molecular Catalysis*. https://doi.org/10.1016/j.mcat.2020.110884
17. Bellardita, M., Yurdakal, S., Tek, B. S., et al. (2021). Tuning the selectivity to aldehyde via pH regulation in the photocatalytic oxidation of 4-methoxybenzyl alcohol and vanillyl alcohol by TiO_2 catalysts. *Journal of Environmental Chemical Engineering*. https://doi.org/10.1016/j.jece.2021.105308
18. Di Paola, A., García-López, E., Ikeda, S., et al. (2002). Photocatalytic degradation of organic compounds in aqueous systems by transition metal doped polycrystalline TiO_2. *Catalysis Today, 75*, 87.
19. Bellardita, M., Augugliaro, V., Loddo, V., et al. (2012). Selective oxidation of phenol and benzoic acid in water via home-prepared TiO_2 photocatalysts: Distribution of hydroxylation products. *Applied Catalysis A, 441–442*, 79–89. https://doi.org/10.1016/j.apcata.2012.07.019
20. Di Paola, A., Bellardita, M., Palmisano, L., et al. (2014). Influence of crystallinity and OH surface density on the photocatalytic activity of TiO_2 powders. *Journal of Photochemistry and Photobiology A, 273*, 59–67. https://doi.org/10.1016/j.jphotochem.2013.09.008
21. Bellardita, M., Garlisi, C., Venezia, A. M., et al. (2018). Influence of fluorine on the synthesis of anatase TiO_2 for photocatalytic partial oxidation: Are exposed facets the main actors? *Catalysis Science and Technology, 8*, 1606–1620. https://doi.org/10.1039/c7cy02382k
22. Hanaor, D. A. H., & Sorrell, C. C. (2011). Review of the anatase to rutile phase transformation. *Journal of Materials Science, 46*, 855–874.
23. Setiawati, E., & Kawano, K. (2008). Stabilization of anatase phase in the rare earth; Eu and Sm ion doped nanoparticle TiO_2. *Journal of Alloys and Compounds, 451*, 293–296. https://doi.org/10.1016/j.jallcom.2007.04.059
24. Zhang, H., & Banfield, J. F. (2000). Understanding polymorphic phase transformation behavior during growth of nanocrystalline aggregates: Insights from TiO_2. *Journal of Physical Chemistry B, 104*, 3481–3487. https://doi.org/10.1021/jp000499j
25. Bellardita, M., Garlisi, C., Ozer, L. Y., et al. (2020). Highly stable defective TiO_2-*x* with tuned exposed facets induced by fluorine: Impact of surface and bulk properties on selective UV/visible alcohol photo-oxidation. *Applied Surface Science*. https://doi.org/10.1016/j.apsusc.2020.145419
26. Wu, Q., Zheng, Q., & van de Krol, R. (2012). Creating oxygen vacancies as a novel strategy to form tetrahedrally coordinated Ti^{4+} in Fe/TiO_2 nanoparticles. *Journal of Physical Chemistry C, 116*, 7219–7226. https://doi.org/10.1021/jp212577g
27. Choudhury, B., Borah, B., & Choudhury, A. (2013). Ce-Nd codoping effect on the structural and optical properties of TiO_2 nanoparticles. *Materials Science and Engineering B, 178*, 239–247. https://doi.org/10.1016/j.mseb.2012.11.017
28. Bansal, J., Tabassum, R., Swami, S. K., et al. (2020). Performance analysis of anomalous photocatalytic activity of Cr-doped TiO2 nanoparticles [Cr(x)TiO2(1–x)]. *Applied Physics A*. https://doi.org/10.1007/s00339-020-03536-z
29. Mazzolini, P., Russo, V., Casari, C. S., et al. (2016). Vibrational-electrical properties relationship in donor-doped TiO_2 by Raman spectroscopy. *Journal of Physical Chemistry C, 120*, 18878–18886. https://doi.org/10.1021/acs.jpcc.6b05282
30. Parker, J. C., & Siegel, R. W. (1990). Calibration of the Raman spectrum to the oxygen stoichiometry of nanophase TiO_2. *Applied Physics Letters, 57*, 943–945. https://doi.org/10.1063/1.104274
31. Fiorenza, R., Bellardita, M., D'Urso, L., et al. (2016). Au/TiO_2-CeO_2 catalysts for photocatalytic water splitting and VOCs oxidation reactions. *Catalysts*. https://doi.org/10.3390/catal6080121
32. Zhu, Q., Peng, Y., Lin, L., et al. (2014). Stable blue TiO_2-x nanoparticles for efficient visible light photocatalysts. *Journal of Materials Chemistry A, 2*, 4429–4437. https://doi.org/10.1039/c3ta14484d
33. Bellardita, M., Di Paola, A., García-López, E., et al. (2013). Send orders for Reprints to reprints@benthamscience.net Photocatalytic CO_2 reduction in gas-solid regime in the presence of bare, SiO_2 supported or Cu-loaded TiO_2 samples. *Current Organic Chemistry, 17*, 2440.
34. Lei, Y., Zhang, L. D., Meng, G. W., et al. (2001). Preparation and photoluminescence of highly ordered TiO_2 nanowire arrays. *Applied Physics Letters, 78*, 1125–1127. https://doi.org/10.1063/1.1350959
35. Serpone, N., Lawless, D., & Khairutdinov, R. (1995). Size effects on the photophysical properties of colloidal anatase TiO_2 particles: Size quantization versus direct transitions in this indirect semiconductor? *The Journal of Physical Chemistry, 99*, 16646–16654. https://doi.org/10.1021/j100045a026
36. Yu, J. C., Yu, Ho., et al. (2002). Effects of F—Doping on the photocatalytic activity and microstructures of nanocrystalline TiO_2 Powders. *Chemistry of Materials, 14*, 3808–3816. https://doi.org/10.1021/cm020027c
37. Bao, Y., Huang, C., Chen, L., et al. (2018). Highly efficient Cu/anatase TiO_2 {001}-nanosheets catalysts for methanol synthesis from CO_2. *Journal of Energy Chemistry, 27*, 381–388. https://doi.org/10.1016/j.jechem.2017.12.015
38. Fiorenza, R., Bellardita, M., Balsamo, S. A., et al. (2022). A solar photothermocatalytic approach for the CO_2 conversion: Investigation of different synergisms on CoO-CuO/brookite TiO_2-CeO_2 catalysts. *Chemical Engineering Journal, 428*, 131249. https://doi.org/10.1016/j.cej.2021.131249
39. Chen, J., Shen, C., Guo, B., et al. (2019). Photocatalytic oxidation of aniline over MO/TiO_2 (M = Mg, Ca, Sr, Ba) under visible light irradiation. *Catalysis Today, 335*, 312–318. https://doi.org/10.1016/j.cattod.2018.11.070
40. Quesada, J., Faba, L., Díaz, E., & Ordóñez, S. (2019). Effect of metal modification of titania and hydrogen co-feeding on the reaction pathways and catalytic stability in the acetone aldol condensation. *Journal of Catalysis, 377*, 133–144. https://doi.org/10.1016/j.jcat.2019.07.029
41. Yurdakal, S., & Augugliaro, V. (2012). Partial oxidation of aromatic alcohols via TiO_2 photocatalysis: The influence of substituent groups on the activity and selectivity. *RSC Advances, 2*, 8375–8380. https://doi.org/10.1039/c2ra20960h
42. Bellardita, M., García-López, E. I., Marcì, G., et al. (2018). Selective photocatalytic oxidation of aromatic alcohols in water by using P-doped g-C3N4. *Applied Catalysis B, 220*, 222–233. https://doi.org/10.1016/j.apcatb.2017.08.033

43. Di Paola, A., Bellardita, M., Megna, B., et al. (2015). Photocatalytic oxidation of trans-ferulic acid to vanillin on TiO_2 and WO_3-loaded TiO_2 catalysts. *Catalysis Today, 252*, 195–200. https://doi.org/10.1016/j.cattod.2014.09.012
44. Palmisano, G., Addamo, M., Augugliaro, V., et al. (2007). Selectivity of hydroxyl radical in the partial oxidation of aromatic compounds in heterogeneous photocatalysis. *Catalysis Today, 122*, 118–127. https://doi.org/10.1016/j.cattod.2007.01.026
45. Niu, X., Yan, W., Zhao, H., & Yang, J. (2018). Synthesis of Nb doped TiO_2 nanotube/reduced graphene oxide heterostructure photocatalyst with high visible light photocatalytic activity. *Applied Surface Science, 440*, 804–813. https://doi.org/10.1016/j.apsusc.2018.01.069
46. Wrana, D., Gensch, T., Jany, B. R., et al. (2021). Photoluminescence imaging of defects in TiO_2: The influence of grain boundaries and doping on charge carrier dynamics. *Applied Surface Science*. https://doi.org/10.1016/j.apsusc.2021.150909
47. Yurdakal, S., Bellardita, M., Pibiri, I., et al. (2021). Aqueous selective photocatalytic oxidation of salicyl alcohol by TiO_2 catalysts: Influence of some physico-chemical features. *Catalysis Today, 380*, 16–24. https://doi.org/10.1016/j.cattod.2021.06.030

Authors and Affiliations

Marianna Bellardita[1] · Mansoor Feilizadeh[2] · Roberto Fiorenza[3] · Salvatore Scirè[3] · Leonardo Palmisano[1] · Vittorio Loddo[1]

[1] Department of Engineering, University of Palermo, Palermo, Italy

[2] Ferdowsi University of Mashhad, Mashhad, Iran

[3] Department of Chemical Sciences, University of Catania, Catania, Italy